Weight-Optimized Structural Antenna Concept for UAS Remote Sensing

Jacob W. Burns[1], Emily J. Arnold[2], and Uday Ballingu[3]
University of Kansas Aerospace Engineering, Lawrence, Kansas, 66045, United States

Radar remote sensing applications for small- to medium-sized UAS have recently been expanded due to the miniaturization of electronic hardware components, but physical limitations associated with the radar antenna continue to make it difficult to meet the very restrictive payload capacities and maximum takeoff weight constraints. One technique that addresses these limitations is to utilize structural antennas, or antennas that serve as a functional aircraft structure, in addition to having sensing capabilities. Designing multi-functional systems and optimizing weight necessitates detailed analysis on the effects of system structural characteristics as well as electrical performance. This paper presents a reduced-weight design for a near-HF antenna that is integrated onto a UAS that balances electrical performance and structural requirements.

I. Nomenclature

BPF	=	blade passage frequency
E	=	elastic modulus
h	=	height
I	=	2nd moment of area (moment of inertia)
k	=	stiffness constant
MPC	=	modal phase collinearity
MS	=	mode shape
rpm	=	revolutions per minute
UAS	=	unmanned aerial systems
VHF	=	very high frequency
ω	=	natural frequency

II. Introduction

Over the last several decades there has been a growing desire to use Unmanned Aerial Systems (UAS) in a variety of geoscience fields for conducting fine resolution earth observations with broader spatial coverage. While there have been significant advancements related to radar electronics miniaturization, the physical limitations related to radar antennas have been hard to overcome, especially at Very High Frequency (VHF) and lower frequencies of operation. Payload limitations are particularly restrictive for small- to medium-scale UAS applications, where the payload is often limited to only a few tens of pounds or less.

The concept of a structural antenna—an antenna that also serves as a load-bearing structure of the airframe—provides structural-sensor synergies that can help overcome the payload limitations of these small vehicles. We recently developed a structural antenna concept for a near-HF radar system that is integrated onto a 55 lbs. helicopter UAS [1]. The radar system, referred to as the "HF Sounder" was developed by the Center for Remote Sensing of Ice Sheets at the University of Kansas for sounding temperate ice in polar regions [2]. The antenna concept is fabricated primarily from carbon fiber reinforced plastic materials given its established conductivity in the VHF range [3] and serves as the landing gear for the vehicle. While this structural-antenna concept is relatively lightweight at 14 lbs. it is slightly above the payload limits of the vehicle, and thus is was desired to further reduce the weight of the antenna.

This paper presents a reduced weight design for the 35 MHz structural-antenna. The lighter weight design was achieved by running a structural optimization analysis. The reduced-weight prototype was then fabricated and both its electrical and structural characteristics were verified via testing. Section III provides an overview of the original design

[1] Graduate Research Assistant, Department of Aerospace Engineering, AIAA Student Member
[2] Assistant Professor, Department of Aerospace Engineering, Senior Member
[3] Graduate Teaching Assistant, Department of Aerospace Engineering, AIAA Student Member

and Section IV presents the results from the verification testing of the original design. Section V and Section VI present the optimized design and its verification testing results, respectively. Finally Section VII outlines the conclusions of the research as well as recommendations for future work.

III. Original Design

A. Design Requirements

The electrical design requirements for the antenna were as follows: 1) a center frequency between 30-40 MHz, 2) be electrically small and lightweight, with the highest possible electrical efficiency, 3) a 10-dB impedance bandwidth of ≥5 MHz, and 4) a gain of ≥ -10 dB across the operational bandwidth [1]. Fig. 1 shows the original antenna prototype. The overall shape of the antenna was driven by the platform it is to be integrated on, namely AeroVironment's Vapor 55 helicopter UAS [4]. The Vapor 55 has a rotor diameter of 90 in., overall length of 100 in., and a payload capacity of 10 lbs. This platform was selected due to its long endurance of 60 minutes, ability to hover, payload capacity, and vertical takeoff and landing capabilities (VTOL) which is ideal for remote field operations [1]. Unlike fixed-wing vehicles, the helicopter lacks long a long wing-structure to support a large antenna, which drove the requirement for the electrically small design.

Given the low speeds and autonomous landing capabilities of the vehicle, the structure was sized by the structural dynamics. The vibrations and downwash from the main rotor can excite potentially hazardous mechanical vibrations in the antenna. For the UAS-integrated antenna concept, the blade passage frequency (BPF) is the primary source of excitation. For a rotor with rotational velocity, n (in rpm), and number of blades, t, the equation for BPF is provided below in Eq. (1).

$$BPF = n * \frac{t}{60} \tag{1}$$

For the Vapor 55 UAS, the main rotor's rotational velocity is 880 rpm, and the number of blades is three, which yields a BPF of 44 Hz. To avoid resonance, it is critical that the natural frequencies of the antenna and integration structure are designed to be at least ±5 Hz from the BPF. Therefore, for a BPF of 44 Hz, the range of unacceptable frequencies is 39 Hz to 49 Hz, which will be referred to as the "keep out zone." Thus in addition to the electrical requirements listed above the antenna was also designed such that the natural frequencies of the antennas are outside of the blade passage frequency of the propulsion system.

B. Overview of Design

Fig. 1 shows the original structural antenna prototype, and Fig. 2 shows the antenna integrated onto the Vapor 55. The overall antenna design is similar to the planar Egyptian ax dipole designs developed by Ziolkowski et al [5], and it consists of an active element located at the center of the larger passive element. The details of the structural antenna design can be found in [1]. The overall diameter of the antenna is 58.6 in. and its height is 5.0 in. The center section of the antenna is manufactured with an I-beam cross section, while the arc sections are manufactured as a "C" cross section. The I-beam is spliced at the center to create the arms of the dipole antenna, but it is reinforced by two fiberglass panels on the top and bottom of the I-beam. The antenna was constructed using wet-layup techniques and AS4 bi-axial plain weave (0°/90°) fabric with DPL 40 epoxy resin. Given that CFRP cannot be soldered to, copper strips were embedded on the exterior of the I-beam laminate in locations where soldering was required between the active and passive elements (shown in the center of Fig. 1). In addition, copper was also embedded in the laminate at the mechanical joints between the center I-beam and arcs. The antenna is fed by soldering a small 50-ohm coax cable to each arm of the antenna, centered on the I-beam web at the splice. As shown in Fig. 2, the antenna is attached to the Vapor 55 via two fiberglass L-brackets that connect to the payload tray at the bottom of the vehicle. In addition, to meet the vibration requirements for the structure, four fiberglass struts were added to connect antenna arcs to the vehicle as well. The struts are connected to the antenna via custom brackets fabricated from aluminum sheet metal. Fiberglass material was used for the struts and center attachment bracket not only for its high stiffness to weight ratio, but also because fiberglass is a dielectric and thus will not ground the antenna to the vehicle. The antenna and integration structures had a total weight of approximately 14 lbs.

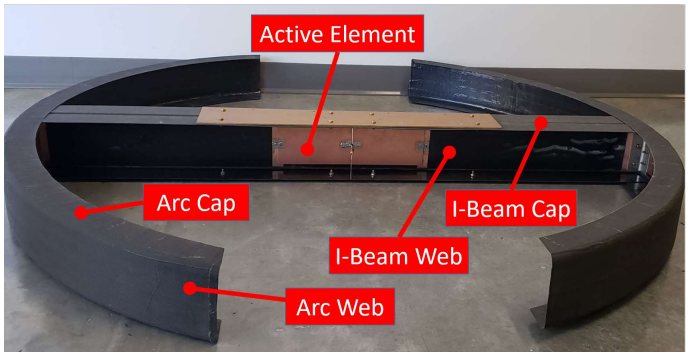

Fig. 1: Fabricated Structural Antenna Prototype

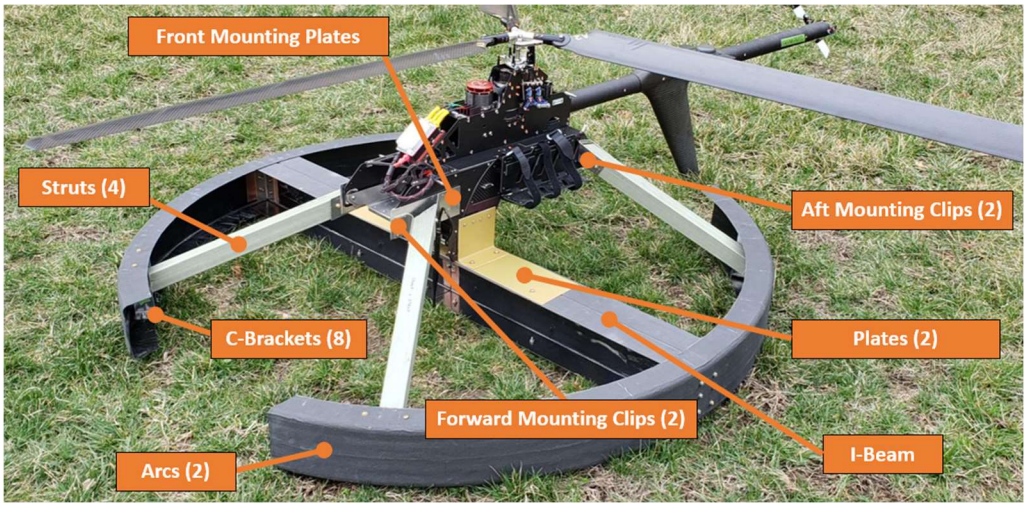

Fig. 2: Antenna-Integrated UAS

IV. Verification of Original Design

A. Finite Element Analysis and Results

As mentioned earlier, the natural frequencies of the structure must not coincide with the blade passage frequency of the main rotor. At resonance, the system undergoes a maximum amplitude response, which can cause potential loss of control or structure failure. In order to predict the antenna structure's natural frequencies, a finite element model of the original antenna design was developed. A modal vibration analysis was performed using MSC Patran/NASTRAN finite element analysis (FEA) software [6] to determine the natural modes of the structure. The geometry of the structure was initially modeled in Siemens NX [7] and subsequently imported into MSC Patran. The materials used in the model are provided in Table 1 and were applied to the corresponding surfaces shown in Fig. 3. The corresponding material properties of each of these materials is provided in Table 2.

Table 1: Original Antenna Material Summary

Component	Material	Total thickness
Arcs	6-ply Biaxial Carbon Fiber	0.0054 in.
I-Beam Cap	6-ply Biaxial Carbon Fiber	0.0054 in.
I-Beam Web	6-ply Biaxial Carbon Fiber	0.0054 in.
Struts	1.5 in. x 1.5 in. Fiberglass	0.125 in.
L-Brackets	6-ply Biaxial Prepreg Fiberglass	0.0606 in.
Plates	6-ply Biaxial Prepreg Fiberglass	0.0606 in.
Mounting Clips	5052-H32 Aluminum	0.050 in.
Mounting Plates	5052-H32 Aluminum	0.050 in.
C-Brackets	7075-T6 Aluminum	0.050 in.

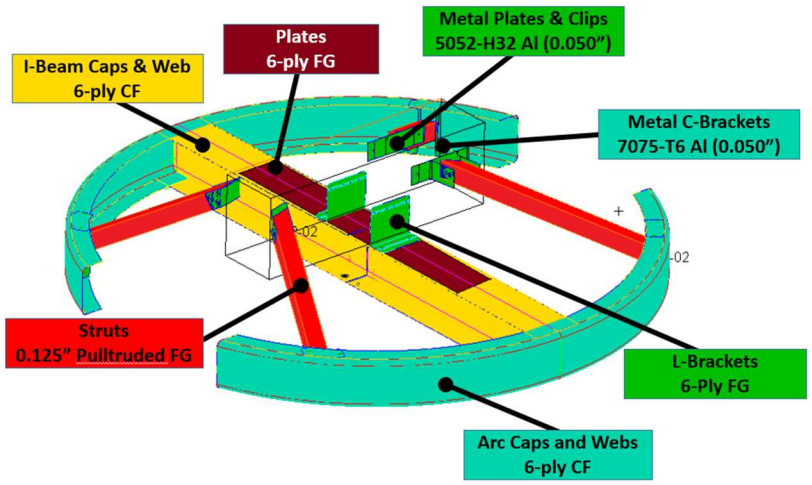

Fig. 3: Property Layout of Original Design

Table 2: Material Properties

MATERIAL	E_{11} (KSI)	E_{22} (KSI)	G_{12} (KSI)	P (LB/IN^3)	POISSON RATIO (~)
AS4/Epoxy, Biaxial Plain Weave, Wet Layup*	9,600	9,100	650	0.059	.032
S-2 Glass 6781/MTM-45 Biaxial Plain Weave Prepreg Fiberglass*	4,320	4,414	710	0.065	0.13
Aluminum**	10,000		3,800	0.098	0.33

*Conservative, open hole allowables were used; **Generic aluminum alloy properties were used for all metal

QUAD4 shell elements were used exclusively in the FEA model. After applying material properties to the appropriate elements, fixed-translation boundary conditions were applied where the system is attached to the UAS. Fig. 4 below shows the meshed FEA geometry along with the fixed boundary conditions (indicated by the light blue markers).

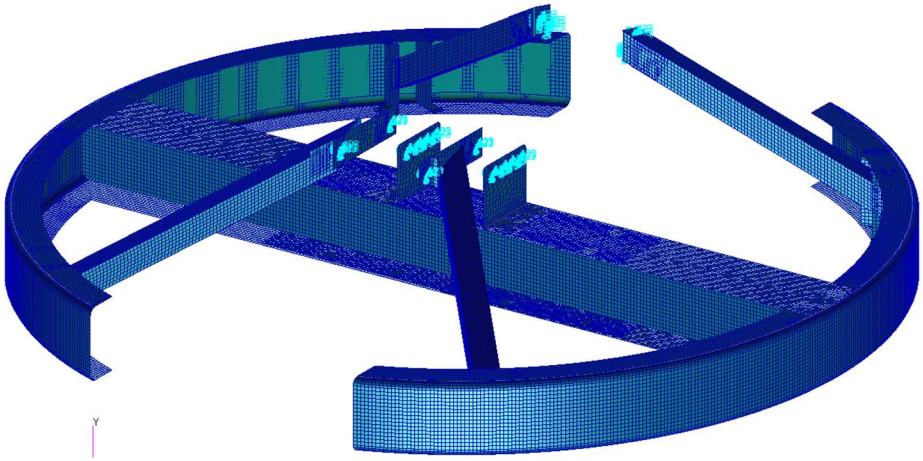

Fig. 4: FEA Model of Antenna Prototype

The first eight mode shapes from the finite element analysis are shown and described below in Table 3. The results showed that the near-resonant frequencies, found in modes 6 and 7, were outside the blade passage frequency of 44 Hz by approximately -5Hz and +7 Hz.

Table 3: First 8 FEA Mode Shapes of Original Design

Mode	Freq. (Hz)	Mode Shape	Description of Mode Shape
1	6.34	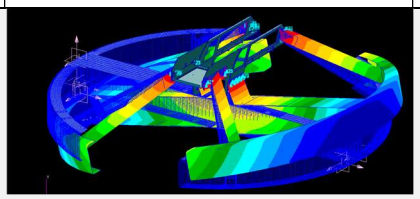	**Rolling (about Z-axis)**
2	23.4	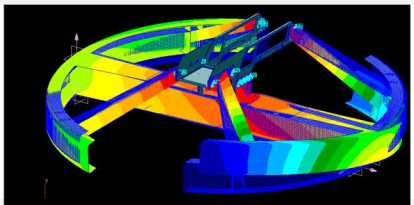	**Left arc yawing (about Y-axis), Right arc pitching (about X-axis)**
3	24.3	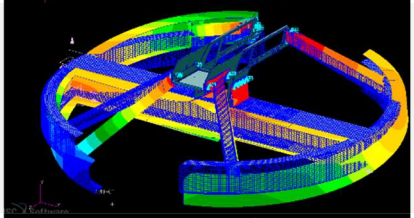	**In-phase pitching (about X-axis)**
4	29.8	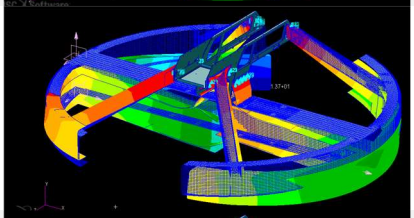	**Left arc pitching (about X-axis), Right arc rolling (about Z-axis)**
5	32.1	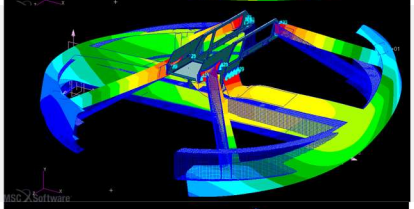	**Out-of-phase pitching (about X-axis)**
6	39.1	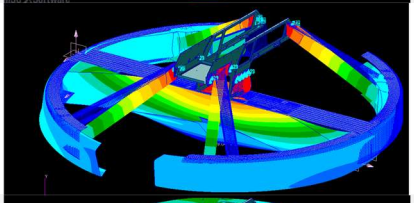	**In-phase yawing (about Y-axis), local compression/tension of arcs**
7	51.7	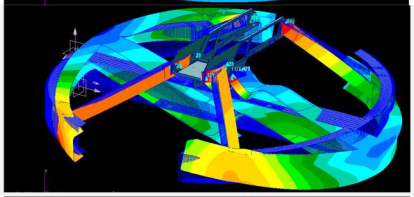	**In-phase rolling (about Z-axis), local compression/tension of arcs**
8	61.2	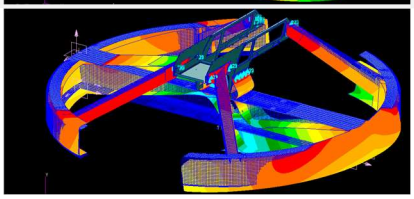	**Out-of-phase rolling (about Z-axis)**

B. Modal Testing

To verify the finite element analysis, an experimental modal analysis was conducted by free-hanging the integrated antenna and vehicle. The excitation source was a pseudorandom vibration induced by a mechanical shaker. Seven accelerometers and one force gauge were connected to the antenna structure as shown in Fig. 5, enabling a series of measurements to be taken to obtain transfer function data. A schematic of the setup of the experimental test is shown below in Fig. 6.

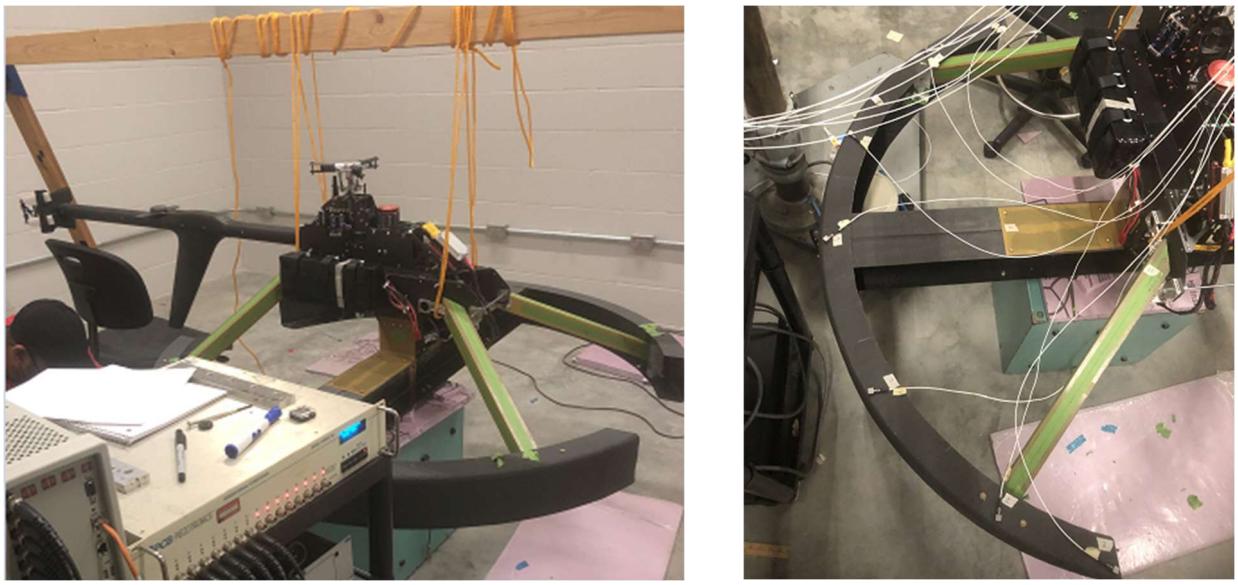

Fig. 5: Experimental Testing: Structure Fixation (left) and Accelerometer Placement (right)

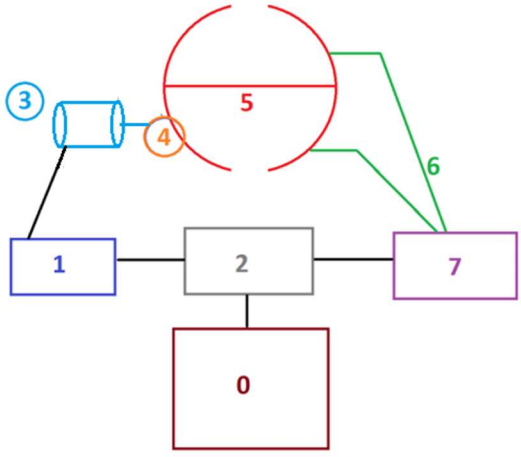

Process	Equipment	Image
0	Workstation (Signal Calc)	
1	Data Physics (Data processing)	
2	Power Amplifier	
3	Force Transducer	
4	Structure	
5	Accelerometers and cables	
6	Signal Conditioner	

Fig. 6 Experimental Setup Schematic (left) and Table of Instruments Used (right)

The experimental test yielded transfer function data, which can be used to find the natural frequencies of the structure as well as the mode shapes. The plot in Fig. 7 shows an example of the resulting transfer functions from the seven accelerometers.

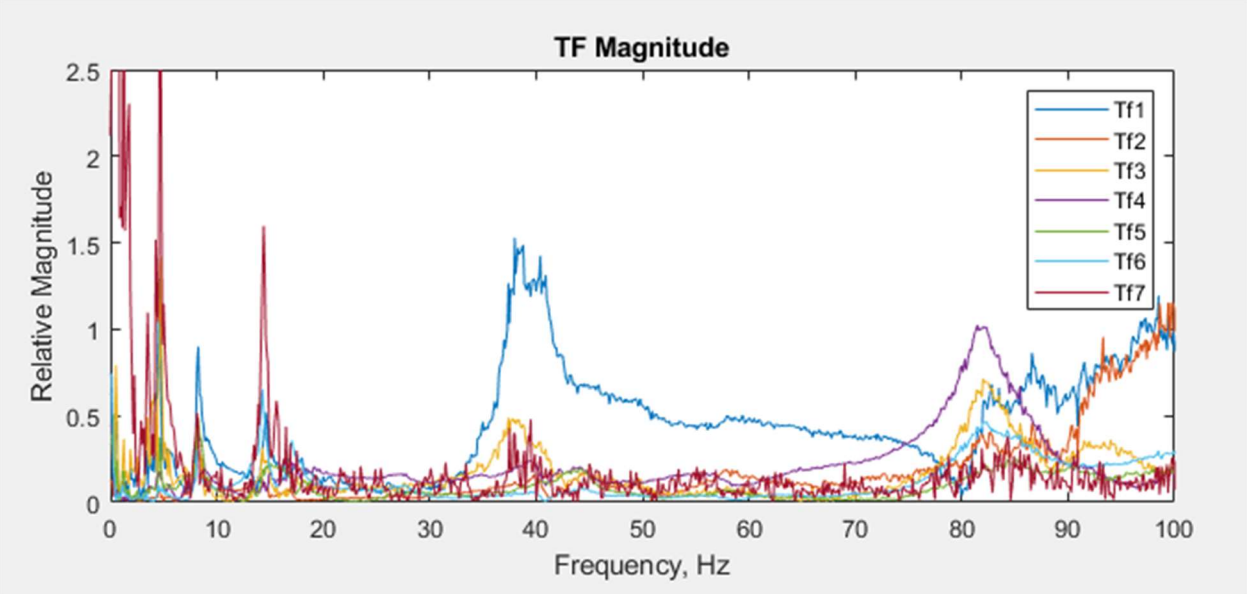

Fig. 7 Transfer Function Results for Original Design

The frequency response function generated by the modal analysis software, ME SCOPE [8], is shown in Fig. 8. The analysis software using data smoothing techniques to limit noise from the experimentation process. Modal characteristics, including frequencies, mode shapes, and Modal Phase Collinearity (MPC) can be determined using the software. The MPC determines how much of a mode is real versus complex based on the eigenvalues of the system's power spectral density matrix. In practice, a high MPC value indicates that the majority of the mode is real-valued and therefore is more likely to show up in a dynamic response. For this first verification of the FEA, mode shapes with MPC values less than 0.8 were disregarded to eliminate many of the modes that were not likely real and were also not of interest since they were outside of the keep out zone. The mode shapes and associated frequencies were determined and summarized in Table 4.

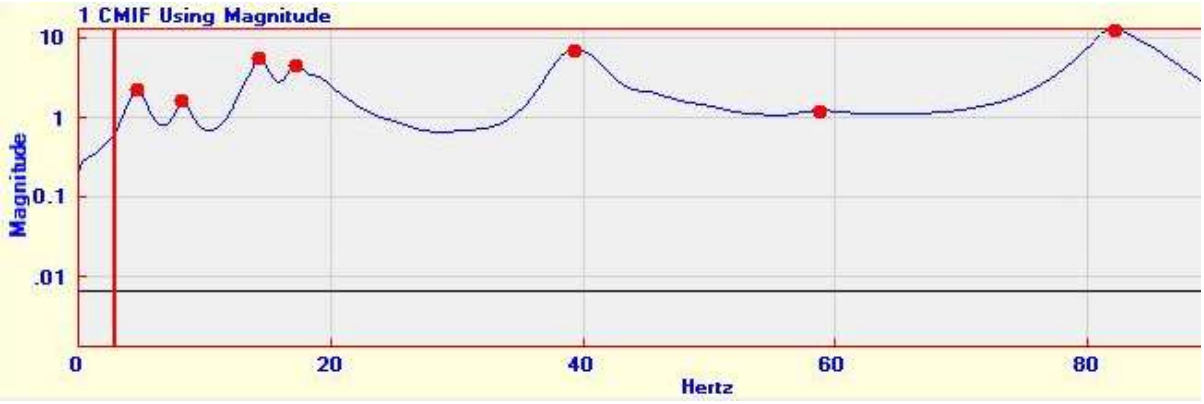

Fig. 8 FRF Results from ME Scope

Table 4: Modal Test Results - Mode Shapes of Original Design

Mode	Freq. (Hz)	Description of Mode Shape
1	**4.49**	**Rolling (about Z-axis)**
2	**8.2**	**Bouncing**
3	**14.3**	**In-phase pitching (about X-axis)**
4	**17.41**	**Out-of-phase pitching (about X-axis)**
5	**39.1**	**Bouncing**
6	**66.3**	**Out of Phase Rolling and Bouncing**
7	**82.5**	**Out-of-phase Rolling (about Z-axis)**

C. Modal Testing: Result Comparison

When verifying a finite element modal analysis with an experimental test, it is most important to consider the similarity of mode shapes, which can also be aided by calculating the MPC of each mode found in the experimental data. This consideration is what helps determine which theoretical modes from the finite element analysis are not significant in practice. The finite element analysis often includes low-energy and/or local modes, which occur when a small part of the structure has an individual dynamic response. Although the finite element analysis can identify these modes, they are not always real modes of concern. In other words, real structures do not always exhibit local modes that can be found in finite element analyses, largely due to the difficulty of accurately modeling boundary conditions and connectivity between structural components. The main focus of the structure is on the global modes, which excite the majority of the structure and can cause loss of control or fatigue.

The nature of each mode shape from the FEA modal analysis was compared and aligned with its corresponding mode from the experimental modal analysis and compared in Table 5 below. Most of the FEA modes had a high error in their natural frequency estimation (greater than 180% in some cases).; however, the overall mode shapes agreed quite well, as did the frequencies of higher frequency modes that were closest to the keep out zone. The closest modal frequencies to the BPF from the experimental results were 39.1 Hz and 82.5 Hz, and each of these were predicted in the FEA within 3% of the experimental results. Not only were the natural frequencies in good agreement, but the mode shapes were very similar as well, indicating a relatively high fidelity of the FEA model (at least in the keep out zone frequency range). It should be noted that the most important part of the FEA and experimental result comparison is the mode shape and frequency agreement within the keep out zone. FEA solutions can have a high degree of variability in modal analysis due to the extremely high dependency on boundary conditions.

Table 5: Comparison of FEA and Experimental Results of Original Design

FEA Mode Shapes		Experimental Mode Shapes	
Freq. (Hz)	**FEA Mode Shape**	**Freq. (Hz)**	**Experimental Mode Shape**
6.34	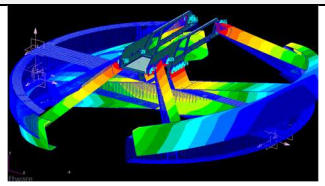	**4.5**	**Rolling (about Z-axis)**
24.3	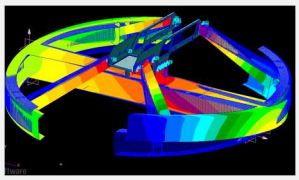	**14.3**	**In-phase pitching (about X-axis)**
32.1	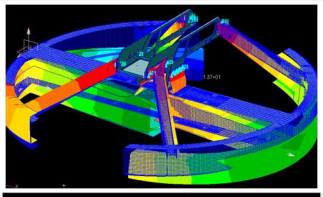	**17.4**	**Out-of-phase pitching (about X-axis)**
39.9	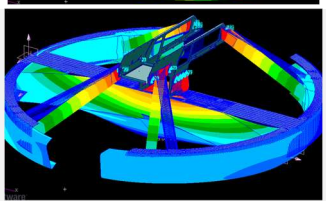	**39.1**	**Bouncing**
84.4	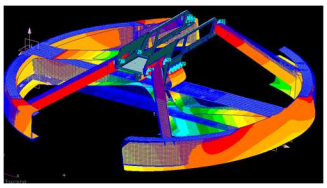	**82.5**	**Out-of-phase Rolling and Bouncing**

D. Anechoic Chamber Testing

The electrical performance of the antenna must also be verified. The original antenna was first designed and simulated in Ansys' High Frequency Simulator Software (HFSS) [9]. After the prototype was fabricated, the antenna was characterized in the University of Kansas's anechoic chamber. Fig. 9 compares the S_{11} of the simulated and measured antennas. The antenna's bandwidth is considered to be where the S_{11} is below -10 dB (called the 10-dB impedance bandwidth). As the plot shows, there was a slight downward shift of ~1MHz in the measured antenna's resonance. This is attributed to the short piece of coax cable that was used to feed the prototype antenna, which effectively increases the electrical length of the antenna and thus reduces the resonance frequency. The bandwidths of the simulated and measured antenna were within 0.5 MHz, and in general, the results are considered to be in good agreement.

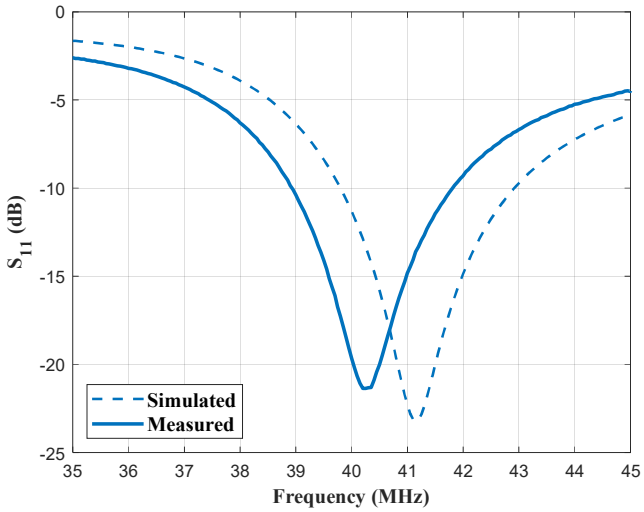

Fig. 9: S_{11} of the Simulated and Measured Antennas

V. Weight-Optimized Design

A. Proposed Weight-Optimized Design

The original design of the antenna was heavier than desired given the 10 lb payload limitation of the vehicle. A weight optimization was not performed for the original antenna in order to expedite fabrication to verify the electrical performance of the new structural antenna concept. A primary contributor for the high weight of the antenna was the use of commercially available fiberglass struts. Long, closed sections are difficult to fabricate using composite hand layup techniques, so commercially available struts were preferred for the initial prototyping stage.

After the electrical performance of the original prototype was shown to match that of physics-based simulations, attention was returned to reducing the weight of the antenna. An initial reduced-weight design was determined manually using Patran/NASTRAN. Once again, the structural dynamics drove the sizing of the antenna. After the manual sizing, an optimization (SOL 200) was performed using NASTRAN. The cap and web thicknesses of the center I-beam, arcs, and fiberglass struts were considered as design variables, and the total weight was the objective to minimize. Using the modal solution from the manual sizing, a constraint was placed on the two closest modes to the keep out zone of 44Hz ± 5Hz (i.e. the first mode below and the first mode above this frequency range). For the carbon fiber antenna, the minimum gage thickness was considered to be three layers while the minimum gage of the fiber glass struts was considered to be two layers. Table 6 summarizes the original thicknesses of the six design variables, their minimum gage, the resultant thickness from the optimization analysis, and the final as-built thickness of the components.

Table 6: Optimization of Laminate Plies and Mapping to Real Thickness

	Original Thickness (# of layers)	Minimum Thickness (# of layers)	Optimization Thickness	Final Thickness (# of layers)
I-Beam Caps	0.054" (6)	0.027" (3)	0.034"	0.036" (4)
I-Beam Webs	0.054" (6)	0.027" (3)	0.043"	0.036" (4)
Arc Caps	0.054" (6)	0.027" (3)	0.027"	0.027" (3)
Arc Webs	0.054" (6)	0.027" (3)	0.027"	0.027" (3)
Strut Caps	0.125"	0.020" (2)	0.020"	0.040" (4)
Strut Webs	0.125"	0.020" (2)	0.020"	0.020" (2)

As the table shows, each variable was limited by the lower bound on the thickness, except the I-beam. These optimized thicknesses were then mapped to realizable thicknesses that also considered manufacturing limitations and efficiencies. The strut caps were increased from a thickness of two layers of fiberglass to four due to the manufacturing approach. To fabricate these components two C-channels were fabricated from the S-2 glass prepreg material and subsequently interleaved together and bonded. Given the minimal weight addition by making the caps of the struts four layers, the optimum thickness was not used for ease of manufacturing. In addition, the caps of the I-beam were thickened to the equivalent thickness of four layers while the webs were thinned to an equivalent of four layers. Again, this was done due to manufacturing considerations for the beams.

The thicknesses in the last column of Table 6 were used in a final FEA modal analysis. From this analysis, the two closest modes to the keep out zone were found to occur at 31 Hz (twisting about the vertical axis) and 50.5 Hz (fore/aft swinging of entire antenna structure). A summary of the weight reduction between the original design and the proposed optimized design is provided below in Table 7.Table 8 To verify these FEA results, the lighter antenna structure was fabricated and subsequently tested. With the new finite element model, the optimized configuration led to an estimated weight savings of about **7.91 lbs.**

Table 7: Weight Reduction Between Models

Model	**Total (FEA) Weight**
Prototype 1 (Built)	13.7 lbs.
Prototype 2 (Proposed)	5.79 lbs.

VI. Verification of Weight-Optimized Design

A. Finite Element Analysis (FEA) Results of Weight-Optimized Design

The same geometry and boundary conditions were used to conduct the FEA of the weight-optimized design. The ply thicknesses of the antenna were updated to a 3-ply layup and the struts were updated to a 2-ply web, 4-ply cap layup. As mentioned, the I-beam was determined to have 4-ply caps and webs given the cured ply thickness of the material. A summary of materials and thicknesses is provided in Table 8 and Fig. 10, and a summary of the FEA modal results are presented in Table 9.

Table 8: Reduced-Weight Antenna Materials Table

Component	Material	Total thickness
Arcs	3-ply Biaxial Carbon Fiber	0.0054 in.
I-Beam Cap	4-ply Biaxial Carbon Fiber	0.0054 in.
I-Beam Web	4-ply Biaxial Carbon Fiber	0.0054 in.
Strut Caps	4-ply Biaxial Prepreg Fiberglass	0.0404 in.
Strut Webs	2-ply Biaxial Prepreg Fiberglass	0.0202 in.
L-Brackets	6-ply Biaxial Prepreg Fiberglass	0.0606 in.
Plates	6-ply Biaxial Prepreg Fiberglass	0.0606 in.
Mounting Clips	6061-T6 Aluminum	0.0320 in.
Mounting Plates	6061-T6 Aluminum	0.0320 in.
C-Brackets	6061-T6 Aluminum	0.0320 in.

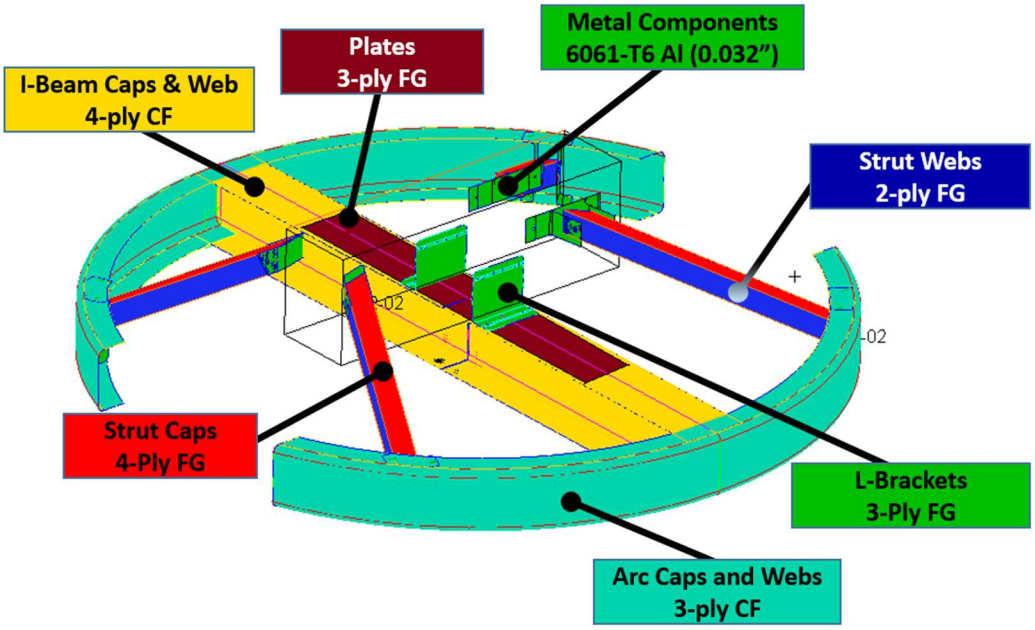

Fig. 10: Property Layout of Optimized Design

Table 9: First 8 FEA Mode Shapes of Optimized Design

Mode	Freq. (Hz)	Mode Shape	Description of Mode Shape
1	11.0	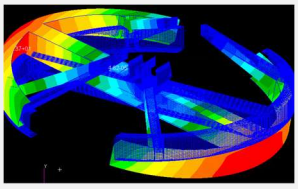	**Rolling (about Z-axis)**
2	18.4	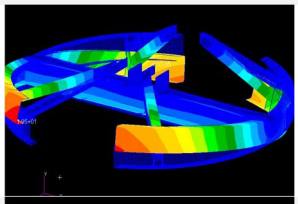	**In-phase pitching**
3	22.1	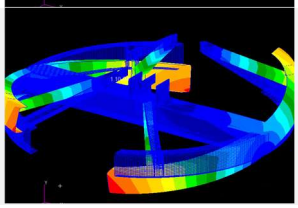	**Out-of-phase pitching (about X-axis)**
4	27.9	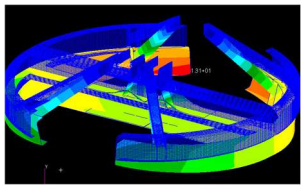	**Bouncing**
5	31.0	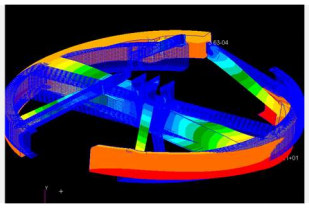	**Out-of-phase pitching (about X-axis)**
6	50.5	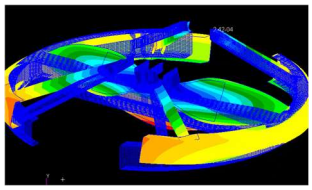	**In-phase yawing (about Y-axis), local compression/tension of arcs**
7	77.8	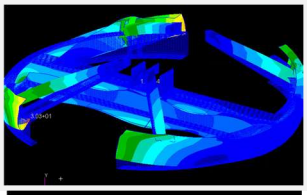	**In-phase rolling (about Z-axis)**
8	78.4	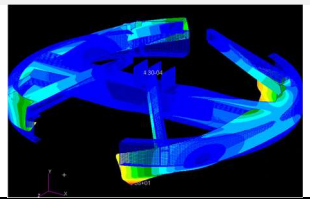	**Out-of-phase rolling (about Z-axis)**

B. Modal Testing of Weight-Optimized Design

To validate the finite element analysis once again, another modal test was conducted using the same setup and procedure as discussed in Section IV.B. The transfer function testing results of the weight optimized design is shown below in Fig. 11.

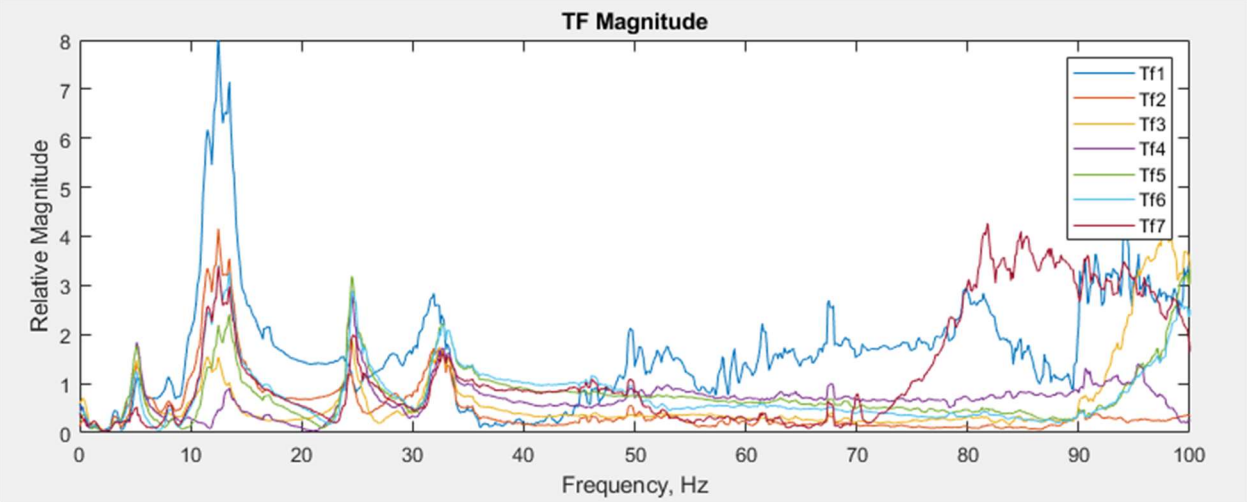

Fig. 11: Transfer Function Results for Optimized Design

The same averaging techniques were used to smooth the data from above to calculate the modal characteristics and mode shapes using ME SCOPE. For this verification, since it is the last experimental test before flight, a more conservative MPC cutoff value of 0.1 was used. This allowed more modes to be considered to ensure each mode analyzed was not discarded until was determined with high confidence to be insignificant. Modal testing results of the weight optimized design are provided below in Table 10 which includes a description of the mode shape.

Table 10: Modal Test Results - Mode Shapes of Optimized Design

Mode	Freq. (Hz)	Description of Mode Shape
1	**5.16**	**Rolling (about Z-axis)**
2	**13**	**In-phase pitching (about X-axis)**
3	**24**	**Bouncing**
4	**25.2**	**Bouncing**
5	**31.2**	**Out-of-phase pitch and bouncing**
6	**48.7**	**Out of phase Local Flex of one Arc**
7	**56.7**	**Flapping**
8	**88.1**	**Out-of-phase rolling**

After examining the mode shapes, frequency response functions, and modal participation factors, it was determined that the two modes closest to the keep out zone which were 48.7 Hz and 56.7 Hz were not significant and were highly likely to be non-real. If possible, one of the best ways to determine if a mode has real energy content is to look at the phase plot of the transfer function. The phase will show a 180˚ shift if there is a mode at that associated frequency. As shown in Fig. 12 below, the phase plot of the transfer function from the experimental results of optimized design has no phase shifts in the keep out zone. There are also no phase shifts in the 50 to 60 Hz frequency band, indicating that both the 48.7 Hz and 56.7 Hz modes are either insignificant (too low of energy to detect) or non-real.

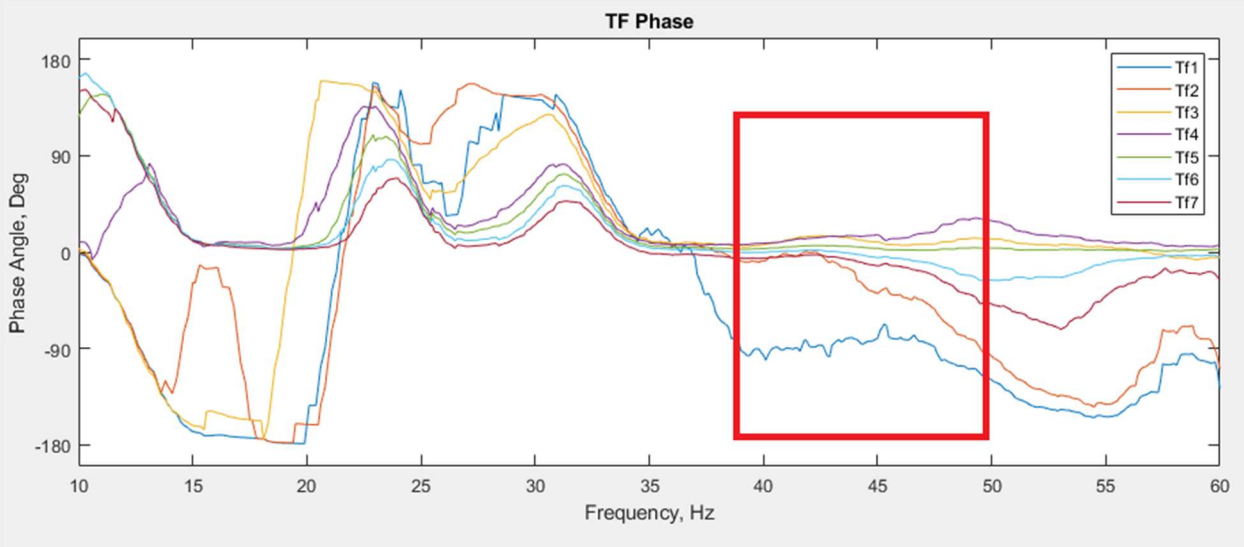

Fig. 12: Phase plot of Transfer Function from Experimental Results of Optimized Design

C. Modal Testing: Result Comparison

The results were compiled by making comparisons were from Table 9 to Table 10, after omitting the modes from Table 10 that were considered insignificant. The test results of the optimized design, including the results in outside of the keep out zone, were quite similar to the results from the FEA of the optimized design. This is largely due to the improvement of modeling of boundary conditions, running multiple analyses in the FEM, doing multiple experimental tests. The resulting mode shapes with the closest frequencies to the keep out zone were 31.2 Hz and 88.1 Hz. The FEA results predicted these frequencies within about a 10% error. Although the two closest frequencies to the keep out zone had a higher error than the original antenna analysis, there was less error across the broader spectrum of modes, indicating an improvement in model fidelity.

Table 11: Comparison of FEA and Experimental Results of Optimized Design

FEA Mode Shapes		Experimental Mode Shapes	
Freq. (Hz)	**FEA Mode Shape**	**Freq. (Hz)**	**Experimental Mode Shape**
11.0	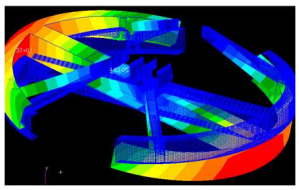	**5.16**	**Rolling (about Z-axis)**
18.4	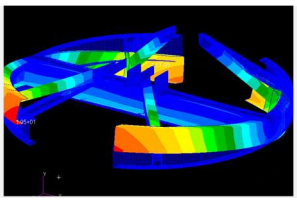	**13**	**In-phase pitching (about X-axis)**
27.9	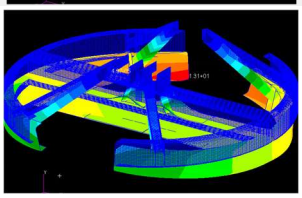	**25.2**	**Bouncing**
31.0	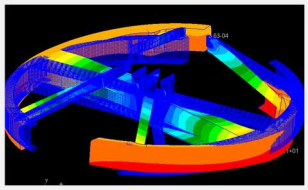	**31.2**	**Out-of-phase pitching and bouncing**
78.4	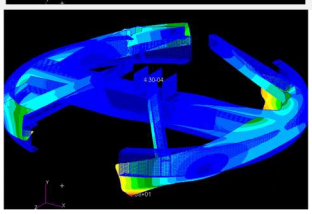	**88.1**	**Out-of-phase rolling**

D. Anechoic Chamber Testing of Optimized Design

After conducting the modal testing, the last step was to verify the electrical performance of the antenna. Fig. 13 compares the S_{11} of the original antenna to the final reduced-weight design. While the updated antenna design had a deeper resonance (indicating a better match), the resonance frequency was within 0.2 MHz and the bandwidth was within 0.5 MHz of the original. Both of these metrics are considered to be in good agreement. The small variations are attributed to the overall variations in manufacturing and not strictly to the reduced thickness of the antenna.

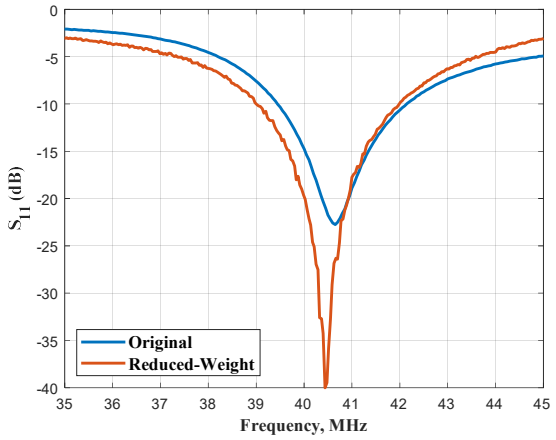

Fig. 13: Comparison of the Original and Reduced-Weight Antenna S_{11}

VII. Conclusion

The design of a reduced-weight structural antenna design for UAS applications was presented. The structural dynamics drove the sizing of the antenna, given the low aerodynamic and inertial loads on the structure. The reduced-weight design was achieved by first tuning the FEA model of the original antenna to the experimental modal results. This FEA model was subsequently used in a NASTRAN optimization to update the thicknesses of the structure to minimize weight. Both the original and reduced-weight antennas were designed to have natural frequencies at least +/- 5 Hz away from the BPF of the vehicle's main rotor (the keep out zone).

The finite element analysis results were more similar to the experimental results for the optimized design than the original design due to improvement of modeling the structure's boundary conditions, as well as taking more experimental data. It should be noted that for high-frequency complex structures, it can be difficult to get a finite element model to be in good agreement with experimental results due to the low stiffness and asymmetric geometry of the as-built prototypes. Despite these obstacles, the original finite element results were within 3% of the experimental frequencies for the two modes closest to BPF, while the results of the optimized design were within 10% for the four closest modes. Further improvement could be made to the finite element model to increase the agreement between the model and the experimental results, namely by more accurately modeling the stiffness and geometric features of the attachment clips from the struts to the vehicle, which play a major role in the finite element results. Although these differences between the finite element model and experiment could be improved upon, the current model and correlating experimental results showed a successful redesign of the antenna and attachment structures that reduced the overall weight and kept the structure's natural frequencies out of the keep out zone.

The optimized antenna weight is less than half of the original design, and is well under the maximum payload capacity of the vehicle. Future work for this project includes integrating the antenna and associated radar hardware and performing extensive flight tests. This system is expected to be deployed over Helheim Glacier in Greenland in Summer 2022.

References

[1] E.J. Arnold, A. Patil, F. Rodriguez-Morales, V. Occhiogrosso, "Near-HF Electrically Small Antenna for UAS Ice-Penetrating Radar," *Microwave and Optical Technology Letters*. Accepted.

[2] Arnold, E. J., Rodriguez-Morales, F., Paden, J., Leuschen, C., Keshmiri, S., Yan, S., Ewing, M., Hale, R., Mahmood, A., Blevins, A., Mishra, A., Karidi, T., Miller, B., and Sonntag, J., "HF/VHF Radar Sounding of Ice from Manned and Unmanned Airborne Platforms," *Geosciences*, Vol. 8, No. 5, May 2018.

[3] Patil, A. S., and Arnold, E. J., "Characterizing Carbon Fiber Conductivity for Structural Antenna Applications," *IEEE Trans. on Antennas and Propag*. *(Early Access)*, doi: 10.1109/TAP.2021.3102037.

[4] AeroVironment Vapor Website, https://www.avinc.com/uas/vapor.

[5] Ziolkowski, R.W., "Low Profile, Broadside Radiating, Electrically Small Huygens Source Antennas," IEEE Access, Vol. 3, 2015, pg. 2644-2650.

[6] MSC Patran/Nastran, MacNeal-Schwendler Corporation, ver. 2018, Stockholm, Sweden.

[7] NX, Siemens NX Software Package 1915, ver. 2019, Munich, Germany.

[8] ME Scope, Visual Modeling Package VT-570, Vibrant Technologies, Centennial, CO. USA.

[9] Ansys® Electromagnetics Suite, ver. 2019.